

Comparison of Multi-Parametric Programming, Mixed-Integer Programming, Gradient Descent Based, Hybrid Minimum Principle, and the Embedding Approach on Six Published Hybrid Optimal Control Examples

Richard T. Meyer, *Student Member, IEEE*, Miloš Žefran, *Senior Member, IEEE*,
and Raymond A. DeCarlo, *Fellow, IEEE*

Abstract—In recent years, the embedding approach for switched optimal control problems has been developed in a series of papers. However, the embedding approach, which advantageously converts the hybrid optimal control problem to a classical nonlinear optimization, has not been extensively compared to alternative approaches. The goal of this paper is thus to compare the embedding approach to multi-parametric programming, mixed-integer programming, gradient-descent based methods, and CPLEX in the context of five recently published examples. The five examples include a spring-mass system, moving-target tracking for a mobile robot, two-tank filling, DC-DC boost converter, skid-steered vehicle. A sixth example, an autonomous switched 11-region linear system, is used to compare a hybrid minimum principle method and traditional numer-

ical programming. For a given performance index for each case, cost and solution times are presented. It is shown that there are numerical advantages of the embedding approach: lower performance index cost, generally faster solution time, and convergence to a solution when other methods fail. In addition, the embedding method requires no ad hoc assumptions (such as predetermined mode sequences) or specialized control models. Theoretical advantages of the embedding approach over the other methods are also described: guaranteed existence of a solution under mild conditions, convexity of the embedded hybrid optimization problem (under the customary conditions on the performance index), solvability with traditional techniques such as sequential quadratic programming avoiding the exponential complexity in number of modes/discrete variables of mixed-integer programming, applicability to affine nonlinear systems, and no need to explicitly label autonomous switches with discrete/mode variables. Finally, some common misconceptions regarding the embedding approach are also addressed including whether it uses an average value control model (no), whether it is necessary to “tweak” the algorithm to obtain bang-bang solutions

R.T. Meyer is with the School of Mechanical Engineering, Purdue University, West Lafayette, Indiana 47907 (email: rt-meyer@purdue.edu).

M.Žefran is with the Department of Electrical and Computer Engineering, University of Illinois at Chicago, Chicago, Illinois, 60607.

R.A. DeCarlo is with the School of Electrical and Computer Engineering Purdue University, West Lafayette, Indiana 47907.

(no), whether it requires infinite switching to implement embedded solution (no), and whether it has real-time capability (yes).

I. HYBRID OPTIMAL CONTROL EMBEDDING APPROACH OVERVIEW

Hybrid and switched systems have modes of operation. Switches can be controlled or autonomous. In much of the literature, all such modes are labeled with discrete variables. Solution of these problems is carried out by a number of algorithms including: multi-parametric programming (MPP) [1], [2], academic [2] and commercial (CPLEX) [3] mixed-integer programming (MIP) implementations, or variants of gradient descent methods [4], [5], [6], [7].

In 2005, an embedding approach was developed by Bengea and DeCarlo [8] and later extended in [9] to a special subclass of autonomous switches. The embedding approach, which converts the switched hybrid optimal control problem to a classical nonlinear optimization, has been successfully used in a variety of applications including power management of hybrid electric vehicles [10] and fuel cell hybrid vehicles [11], mobile robot slip control [12], and real-time switching control of DC-DC converters [13], [14], [15], [16].

The goal of this paper is to evaluate the convergence time, resulting performance index costs, and requirements (e.g., requisite assumptions) of these approaches and algorithms in the context of six published examples:

- (i) spring-mass system [1],
- (ii) a mobile robot [4],
- (iii) two-tank system [5],
- (iv) a dc-dc boost converter [17],
- (v) skid-steered vehicle [18], [19], and
- (vi) autonomously switched system with 11 state space regions [6], [7].

In example (i) we compare the embedding approach to MPP, MIP, and CPLEX. For examples (ii) and (iii) we compare the embedding method to gradient descent based methods in [4], [5], and in example (iv) we compare the embedding approach with the available information in [17] and MPP, MIP, and CPLEX [3] results. In example (v) we show that approach in [18], [19] is an application of the embedding approach and hence we replicate their results. Finally, for example (vi) we show that the approach in [9] which reduces the autonomous switched problem to a traditional numerical programming problem favorably compares to the minimum principle solution approach in [6] that utilizes discrete states to describe the autonomous switches.

The work shows definitively that the embedding method is not only easier to implement, but usually faster, achieves universally lower costs, and avoids, in the cases above, the use of simplifying assumptions. Specifically, the embedding approach does not require the use of scheduled switching, the generation of off-line maps, and ad hoc assumptions on continuous time control such as a single constant control over extended prediction horizons [17]. For nonlinear affine systems, the embedding method does not need a piecewise linear-affine approximation as is done in [1], [17]. Finally, in the latest implementation of the MPP method [2] the authors caution against using general nonlinear models; with the embedding method all that is required is that the control system be affine. In addition, the embedding approach theoretically guarantees the existence of a solution assuming appropriate convexity of the integrand of the performance index and an affine control system.

A. Embedding Approach Description

Details of the embedding method have been set forth in [8], [9], [10], [11], [20], [21], [22]. We first address

the relationship of the embedded model to the switched model, and then switched and embedded optimal control problems. In the embedding approach to hybrid optimal control one forms the embedded model, for example, of a two switched system: $\dot{x} = (1 - v)f_0(t, x, u_0) + vf_1(t, x, u_1)$. Here v is a control determined to meet some objective and u_0 and u_1 are the continuous time controls in modes 0 and 1, respectively. In the embedded model one allows v to take values in the interval $[0, 1]$; in the switched model v takes values in the set $\{0, 1\}$. Note that in the switched model, u_0 and u_1 cannot be active at the same time and are replaced by a single continuous time control u . One notes that EVERY trajectory of the switched model is a trajectory of the embedded model. Indeed it has been shown in [8] that the switched trajectories are DENSE in the set of embedded system trajectories. One then defines an integral performance index (standard fare) whose integrand is the convex combination of each mode's performance integrand; the convex combination is analogous to that of the embedded model. Each integrand is required to be convex in the continuous control. It is important to emphasize that it has been proved in [8] that the embedded optimal control problem (EOCP) always has a solution for any affine control system assuming the convexity of the integrand in the continuous-time controls; no similar results exist in the hybrid optimal control literature.

If the switched optimal control problem (SOCP) has a solution, it is a solution of the EOCP except possibly in the following isolated case: there is a terminal constraint set and an optimal solution reaches the terminal constraint set at a point on its boundary. In this rare and easily fixed case, it is possible (but not necessarily true) that the SOCP solution is bounded away from the solution to the EOCP; in this case, the SOCP cost is bounded above the EOCP cost. The "fix" is to simply

cover the terminal state constraint set with a slightly larger open set; this would result in a "new" SOCP solution with cost equal to the EOCP solution. The only example in this paper with a terminal constraint set is in Section II-A, a spring mass system, and we construct a switched solution via the embedding approach meeting the terminal conditions with a cost lower than MPP as published in [1] and MIP solutions from the multi-parametric toolbox (MPT) [2] and CPLEX [3].

Thus for the models studied in the examples of this paper, the EOCP always has a solution and if the associated SOCP has a solution, the SOCP solution is one of the possibly non-unique solutions given by the optimal solution space of the EOCP. The SOCP may not have a solution in the sense that there is no minimum of the performance index over the set $\{0, 1\}$ due for example to constraints: the EOCP solution is the infimum over the set $\{0, 1\}$ in that case. (Thus the MPP and MIP approaches are infeasible when there does not exist a solution.) Only when there does not exist a SOCP solution would one approximate the EOCP solution with a switched solution using finite time switching; this is always possible since the switched system trajectories are DENSE in the embedded system trajectories. Bengea and DeCarlo [8] provide a construction for approximating the EOCP solution with an SOCP trajectory to any given precision using the Chattering Lemma; practically speaking the duty cycle interpretation is often adequate. A brief study of projection methods is set forth in [23]. All duty cycle interpretations only require finite time switching. Finally, we point out that when the SOCP does NOT have a solution, i.e., the performance index does not have a minimum over the class of switched systems, the costs associated with the embedded solution and the projection of that solution via a duty cycle interpretation onto the feasible set $\{0, 1\}$, (PWM solution)

are virtually identical [13], [15], [16].

In general, the SOCP is NOT convex. The EOCP is convex over rather general conditions set forth in Bengea and DeCarlo [8] which are satisfied by the formulations in this paper. If the SOCP does not have a solution as described previously, then mixed-integer programming approaches are ill-posed. On the other hand, since the EOCP is convex and there are no integer variables (even in the presence of autonomous switches) and since it always has a solution under very reasonable conditions, the EOCP can be solved using classical nonlinear programming techniques such as SQP. One of the observations of this paper is that MIP methods fail even for some of the simple examples tested here; instead the embedding approach always finds a solution and is usually faster.

B. Common Concerns about the Embedding Approach

One common misconception is that the embedding method averages the vector fields of the switched system similar to the Filippov method in variable structure control (VSC). In VSC, Filippov's method is used to determine a solution to a differential equation whose right hand side is discontinuous on a sliding manifold or discontinuity surface due to infinitely fast switching in the control. Filippov's method takes a convex combination of two vector fields $(1-\alpha)f^+ + \alpha f^-$ and chooses the variable α to achieve an "average" value consistent with a tangent plane to the discontinuity surface [24]. This is not the case in the embedded optimal model where the equivalent of α is a control variable to be chosen so that a performance metric is minimized.

Similarly, the boost and buck converter literature considers time scale separation and linearization about an operating point(s) to obtain an "average value model". On the other hand, the embedding method uses the

original model and simply forms a convex combination of the vector fields to create a solution space in which the original problem can be solved. Nowhere is the model averaged in regards to time scales or operating points [13], [14], [15], [16].

Another question that has arisen is how one guarantees that a bang-bang solution is generated by the optimization algorithm? In general, it is not necessary to tweak the algorithm. Non-bang-bang solutions in for example a 2 mode system require that the Hamiltonians in each mode of operation be equal numerically [8]; that situation occurs rarely in general but more often when constraints are imposed on the switching set which must remain convex, as in the work of this paper. In a 3 mode or greater system such as in [23], two or more Hamiltonians can be equal, but if one of the many is "larger", then the solution is bang-bang. However, as stated above, bang-bang solutions are not necessary since non-bang-bang solutions can always be approximated arbitrarily well with bang-bang solutions.

Another issue is EOCP solutions where v is not in the set $\{0, 1\}$. A value of v that minimizes the performance index in the interior $(0, 1)$ does NOT mean that the SOCP does not have a solution or that infinite switching is required to implement the solution. In [8], the value of v is computed for the example in [25] which is shown to have an infinite number of bang-bang solutions for $v = 0.5$. In that example, $v = 0.5$ is shown to mean that one must spend equal amounts of time in each mode. Thus a duty cycle interpretation often used for a projection method is consistent with KNOWN theoretical properties [8].

Further, why is such a solution, $v = 0.5$, considered singular? Because the Hamiltonians associated with each mode are equal causing a specific function (within a convex combination of the Hamiltonians) given in [8]

to be identically zero on a time interval of non-zero measure. Equal Hamiltonians and existence of solutions were not considered in, e.g., [26], [27].

A comment similar to others discussed above argues that the method allows one to use classical sequential quadratic programming, or that the embedding problem is nothing more than a classical nonlinear optimization. As pointed out above, that is precisely why one wants to use the embedding method, because it completely avoids the combinatorial complexity of mixed-integer programming. As we will see in the examples to follow, mixed-integer programming is generally slow and often does not converge.

In the MPP applications, one does offline computation and then creates look-up tables specific to a model and set of objectives. Look-up table approaches cannot deal with changes in parameters or control objectives, and hence fail to have the real time capability of the embedding approach reported, for example, in [13].

A conclusion of this work is that for the methods studied in this paper excluding the embedding approach, not only are there convergence issues for medium horizon windows, but when the programs do give an answer, the computation time is possibly orders of magnitude larger than the embedding method.

II. HYBRID OPTIMAL CONTROL EXAMPLES

In this section, the embedding approach for hybrid optimal control (HOC) is applied to a spring-mass hybrid system [1], a switched-mode mobile robot [4], a two-tank hybrid system [5], a DC-DC boost converter [17], and a skid-steered vehicle [18], [19]. The results from the embedding approach are compared to those from MPP [1], MIP/MPT (MIP using the MPT), MIP using CPLEX, a method that computes switching times for a pre-determined mode sequence [4] as well as a follow-on

approach that additionally finds the mode sequence [5]. Appendix A outlines the MATLAB-based embedding approach solution algorithm used herein. Space considerations preclude detailed descriptions of the optimal control problem solution methods compared to the embedding approach, however each is briefly presented in the example it is first used in. Finally, as set forth in [9], traditional numerical methods are applied to an 11 autonomous mode linear system [6], [7]. Passenburg et al. apply a hybrid minimum principle [6], [7] to the problem and by formally labeling autonomous modes explicitly account for transitions across discontinuity surfaces.

In the following examples, the term “mode” indicates a dynamical vector field selected with a discrete control input. However, “mode” has been used in the past to indicate both controlled and uncontrolled (autonomous) switching of vector fields. Herein, we term the use of “mode” resulting from an autonomous switch as an “autonomous-mode” or “a-mode”. In [9], [21], it was shown that including autonomous switches in the mode definitions is unnecessary for the embedding approach and control problems with only autonomous switches need no mode designations and are solvable with traditional numerical programming.

Further, in each of the examples we use the terms “numerical optimization cost” and the “simulation cost”. By numerical optimization cost we mean the cost computed via the numerical optimization program using collocation and trapezoidal numerical integration of the PI; by simulated cost we mean the cost obtained by numerically integrating the system ODE’s using the piecewise constant continuous controls from the numerical optimization.

In all of the examples, the EOCP is solved using MATLAB’s *fmincon* function following the general procedure outlined in Appendix A. Using a numerically superior solver would only improve the convergence rate and

solution times of the results reported for the EOCP. All the code used to generate the results in this paper can be accessed at [28].

A. Spring-Mass Hybrid System [1]

Example 14.2 in [1] introduces the spring-mass hybrid optimal control problem. A mass is connected to ground with a spring in series with a damper that represents viscous friction. The spring has affine characteristics and the viscous friction coefficient can be changed from one value b_1 to a different value b_2 instantaneously with a binary input. The continuous-time spring-mass system dynamics are

$$\begin{aligned} \dot{x}_1(t) &= x_2(t) \\ M\dot{x}_2(t) &= -k(x_1(t)) - b(u_2(t))x_2(t) + u_1(t) \end{aligned} \quad (1)$$

where the the spring coefficient $k(x_1(t))$ and viscous friction coefficient $b(u_2(t))$ are

$$k(x_1(t)) = \begin{cases} k_1x_1(t) + d_1, & x_1(t) \leq x_m \\ k_2x_1(t) + d_2, & x_1(t) > x_m \end{cases} \quad (2)$$

$$b(u_2(t)) = \begin{cases} b_1, & u_2(t) = 1 \\ b_2, & u_2(t) = 0 \end{cases} \quad (3)$$

with x_1 and x_2 the mass position and velocity, respectively; the system has two modes and two a-modes. System parameters are given as $M = 1$, $b_1 = 1$, $b_2 = 50$, $k_1 = 1$, $k_2 = 3$, $d_1 = 1$, $d_2 = 7.5$, and $x_m = 1$. The spring-mass example is solved using MPP (the original solution approach in [1]), mixed-integer programming with both MIP/MPT and CPLEX, and the embedding approach. MPP [1], [2] solves the optimization problem offline for a full range of initial state values to obtain explicit state-feedback controllers. The optimal state-feedback control for a linear piecewise affine (PWA) control model (as used with MPP here) is a PWA

function of the initial state with controller parameters defined on polyhedron partitions of the feasible state space, i.e., the controller parameters are taken from a look-up table with initial state input.

To implement the MPP algorithm in [1], four ‘‘modes’’ were defined depending on the discrete input u_2 and spring coefficient of (2); the ‘‘modes’’ are a mixture of both modes in the sense used here and a-modes. The dynamics in each ‘‘mode’’ are discretized with a 0.5 time unit sampling resulting in a discrete-time PWA system:

$$\begin{aligned} x(k+1) &= \begin{cases} A_1x(k) + B_1u_1(k) + f_1, & x_1(k) \leq 1, u_2(k) \leq 0.5 \\ A_2x(k) + B_2u_1(k) + f_2, & x_1(k) > 1, u_2(k) \leq 0.5 \\ A_3x(k) + B_3u_1(k) + f_3, & x_1(k) \leq 1, u_2(k) \geq 0.5 \\ A_4x(k) + B_4u_1(k) + f_4, & x_1(k) > 1, u_2(k) \geq 0.5 \end{cases} \end{aligned} \quad (4)$$

where A_i , B_i , and f_i are listed in [1]. The MPP control objective is to minimize

$$\begin{aligned} J_m(x(0), U_0, N) &= x(N)^T Px(N) \\ &+ \sum_{k=0}^{N-1} x(k)^T Qx(k) + u(k)^T Ru(k) \end{aligned} \quad (5)$$

over $U_0 = [u(0)^T, \dots, u(N-1)^T]^T$ ($u(k) = [u_1(k), u_2(k)]^T$) and subject to (4), $x_1, x_2 \in [-5, 5]$, $u_1 \in [-10, 10]$, and a terminal state constraint set $\mathcal{X}_f \in [-0.01, 0.01] \times [-0.01, 0.01]$. The performance index parameters are $N = 3$, $P = Q = I_2$, $R = \begin{bmatrix} 0.2 & 0 \\ 0 & 1 \end{bmatrix}$ and the initial state is $x(0) = [3, 4]^T$. The MPP problem is solved using MPT routines in MATLAB. Furthermore, the MPP problem formulation is also solved with both MIP/MPT and CPLEX. The MIP/MPT problem is also solved with MPT routines in MATLAB. For the CPLEX problem, CPLEX’s convex quadratic performance index optimizer, subject to linear constraints, is called from

MATLAB.

Next, the embedding approach problem is set forth. First, the continuous-time embedded model is formed using two modes (recall the embedding approach does not define separate modes based on autonomous switching [9], i.e., have a-modes).

$$\begin{aligned} \dot{\tilde{x}}(t) = & (1 - \tilde{v}(t)) \begin{bmatrix} \tilde{x}_2(t) \\ -k(\tilde{x}_1) - b_2\tilde{x}_2(t) + \tilde{u}_1^0(t) \end{bmatrix} \\ & + \tilde{v}(t) \begin{bmatrix} \tilde{x}_2(t) \\ -k(\tilde{x}_1) - b_1\tilde{x}_2(t) + \tilde{u}_1^1(t) \end{bmatrix} \end{aligned} \quad (6)$$

where $(\tilde{\cdot})$ is an embedded system value, $\tilde{v} \in [0, 1]$ is the embedded mode switch value and \tilde{u}_1^0 and \tilde{u}_1^1 are the continuous controls in each mode. Notice that $\tilde{v} = 0/\tilde{v} = 1$ in (6) corresponds to $u_2 = 0/u_2 = 1$ in (1). The embedded problem is

$$\min_{\tilde{u}_1^0, \tilde{u}_1^1, \tilde{v}} J_E(x(t_0^p), \tilde{u}_1^0, \tilde{u}_1^1, \tilde{v}, t_0^p, t_f^p) \quad (7)$$

where $[t_0^p, t_f^p]$ is the prediction interval and

$$\begin{aligned} J_E = & \int_{t_0^p}^{t_f^p} \left\{ \tilde{x}(t)^T Q_E(t) \tilde{x}(t) \right. \\ & + (1 - \tilde{v}(t)) \begin{bmatrix} \tilde{u}_1^0(t) & 0 \end{bmatrix} R_E(t) \begin{bmatrix} \tilde{u}_1^0(t) \\ 0 \end{bmatrix} \\ & \left. + \tilde{v}(t) \begin{bmatrix} \tilde{u}_1^1(t) & 1 \end{bmatrix} R_E(t) \begin{bmatrix} \tilde{u}_1^1(t) \\ 1 \end{bmatrix} \right\} dt, \end{aligned} \quad (9)$$

with the minimization subject to (6), the previously defined bounds on the states and continuous control input, and terminal state constraint set. To solve the embedded optimal control problem numerically, the discretized system representation in (4) is reformulated in

the embedded context as

$$\begin{aligned} \tilde{x}(k+1) & = \begin{cases} (1 - \tilde{v}(k)) [A_1\tilde{x}(k) + B_1\tilde{u}_1^0(k) + f_1] \\ + \tilde{v}(k) [A_3\tilde{x}(k) + B_3\tilde{u}_1^1(k) + f_3], & \tilde{x}_1(k) \leq 1 \\ (1 - \tilde{v}(k)) [A_2\tilde{x}(k) + B_2\tilde{u}_1^0(k) + f_2] \\ + \tilde{v}(k) [A_4\tilde{x}(k) + B_4\tilde{u}_1^1(k) + f_4], & \tilde{x}_1(k) > 1 \end{cases} \end{aligned} \quad (10)$$

and the trapezoidal numerical integration representation of (9) is

$$\begin{aligned} \hat{J}_E = & \tilde{x}(N)^T P \tilde{x}(N) + \sum_{k=0}^{N-1} \left\{ \tilde{x}(k)^T Q \tilde{x}(k) \right. \\ & + (1 - \tilde{v}(k)) \begin{bmatrix} \tilde{u}_1^0(k) & 0 \end{bmatrix} R \begin{bmatrix} \tilde{u}_1^0(k) \\ 0 \end{bmatrix} \\ & \left. + \tilde{v}(k) \begin{bmatrix} \tilde{u}_1^1(k) & 1 \end{bmatrix} R \begin{bmatrix} \tilde{u}_1^1(k) \\ 1 \end{bmatrix} \right\} \end{aligned} \quad (11)$$

where $Q_E(t - t_0^p)$ and $R_E(t - t_0^p)$ were chosen such that (11) is equivalent to (5). If $\tilde{v}(k) \in (0, 1)$, then mode and control projection are required. Here, the projection method of [11], [23] is applied where the projected mode, \hat{v} , is zero if $\tilde{v} \leq 0.5$ and one otherwise. The projected control \hat{u}_1 is equal to $(1 - \tilde{v})\tilde{u}_1^0$ if $\hat{v} = 0$ and $\tilde{v}\tilde{u}_1^1$ if $\hat{v} = 1$.

Figs. 1 and 2 shows the state trajectories and evolution of the continuous and discrete controls for the embedding approach and MPP; MIP/MPT and CPLEX results are nearly identical to the MPP results and not shown. The embedding approach results in 3 mode projections over 25 partitions. The projections occurred on the intervals $[0.5, 1]$, $[1, 1.5]$ and $[12, 12.5]$. In all cases, the embedded mode value was less than approximately 0.3, which implies that the mode value was projected to 0. Table I lists the performance index costs, J , and control solution times, Δt^r , for the simulation associated with $N = 3$ plus simulations with $N = 4$ with $t_s = 0.375$

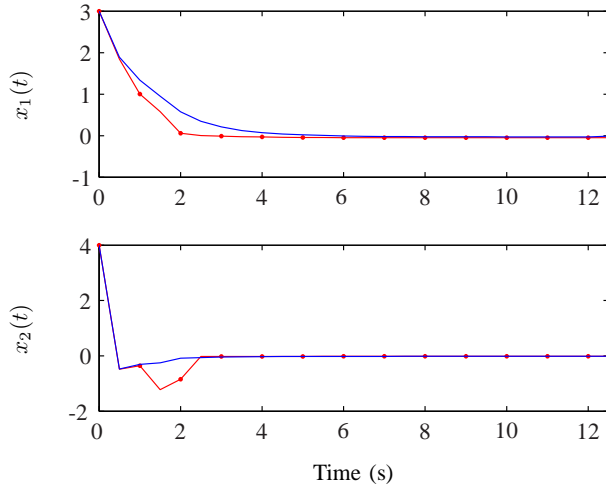


Fig. 1. Spring-mass example state responses: (—) EOC with projection, (•) MPP (MIP/MPT and CPLEX have similar results).

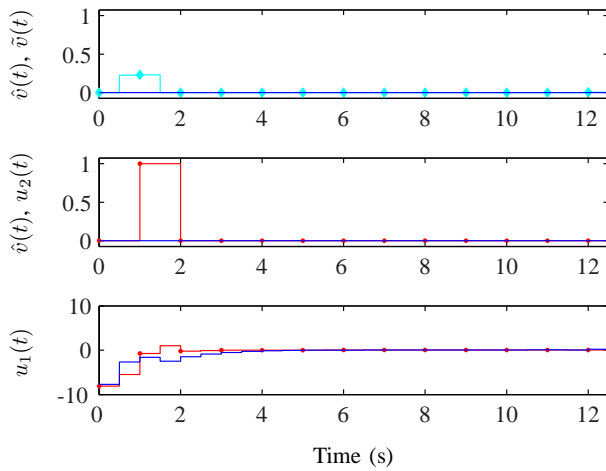


Fig. 2. Spring-mass example continuous and discrete controls: (—) EOC with projection, (◆) EOC without projection, (•) MPP (MIP/MPT and CPLEX have similar results).

and $N = 5$ with $t_s = 0.3$. There are 10 mode projections over 33 partitions needed for $N = 4$ and 7 over 42 partitions for $N = 5$. We conclude that for the same performance metrics and the same example, the embedding approach achieved lower costs in all trials. Furthermore, for a model predictive control (MPC) window of 5 partitions, the embedding approach was 143 times faster than the MIP/MPT approach and 22

TABLE I
SPRING-MASS EXAMPLE EOC (WITH AND WITHOUT PROJECTION), MPP, MIP/MPT, CPLEX PERFORMANCE INDEX COST, J , AND SOLUTION TIMES, Δt^r , FOR THE SIMULATION.

Metric	$N = 3$	$N = 4$	$N = 5$
	$t_s = 0.5$	$t_s = 0.375$	$t_s = 0.3$
J_E , proj.	47.91	62.38	85.65
J_E , no proj.	47.50	59.70	71.67
J_{MPP}	53.90	72.84	89.35
$J_{MIP/MPT}$	53.81	72.78	89.35
J_{CPLEX}	53.89	72.84	87.73
Δt_E^r , proj.	3.86s	9.42s	9.99s
Δt_E^r , no proj.	3.81s	7.78s	8.75s
Δt_{MPP}^r	9.31s	31.20s	222.55s
$\Delta t_{MIP/MPT}^r$	33.73s	72.78s	1434.7s
Δt_{CPLEX}^r	1.00s	2.12s	3.20s

times faster than the MPP approach. Although the MPP approach generates a look-up table, if any parameters change or there are modeling issues, the entire table must be recomputed. The embedding approach was on average about 3.5 times slower than using CPLEX. CPLEX is not a general purpose minimization program like *fmincon* that we use to solve the EOCP. CPLEX is specifically tailored to minimize a quadratic cost function subject to linear equality constraints (as is the spring-mass problem).

B. Mobile Robot Hybrid System [4]

Wardi et al. [4] consider the problem of a mobile robot tracking a moving target while avoiding obstacles. The robot has three operating modes: go to goal (G2G), avoid obstacle 1 (Avoid1), and avoid obstacle 2 (Avoid2). The robot's dynamic equation of motion is

$$\dot{x}(t) = \begin{bmatrix} V \cos(x_3(t)) \\ V \sin(x_3(t)) \\ u - x_3(t) \end{bmatrix} \quad (12)$$

where V is

$$V = \begin{cases} \bar{V}, & \|x_R - x_G\| \geq r \\ \frac{\bar{V}}{r} \|x_R - x_G\|, & \|x_R - x_G\| < r \end{cases} \quad (13)$$

and u is defined for the three modes as

$$u_{G2G} = \tan^{-1} \left(\frac{x_{G,2}(t) - x_{R,2}(t)}{x_{G,1}(t) - x_{R,1}(t)} \right) \quad (14)$$

$$u_{Avoid1} = \begin{cases} \phi_\Phi - \pi/2, & \phi_\Phi - x_3 \geq 0 \\ \phi_\Phi + \pi/2, & \phi_\Phi - x_3 < 0 \end{cases} \quad (15)$$

$$u_{Avoid2} = \begin{cases} \phi_\Psi - \pi/2, & \phi_\Psi - x_3 \geq 0 \\ \phi_\Psi + \pi/2, & \phi_\Psi - x_3 < 0 \end{cases} \quad (16)$$

and ϕ_Φ and ϕ_Ψ are

$$\phi_\Phi = \tan^{-1} \left(\frac{x_{\Phi,2} - x_{R,2}(t)}{x_{\Phi,1} - x_{R,1}(t)} \right) \quad (17)$$

$$\phi_\Psi = \tan^{-1} \left(\frac{x_{\Psi,2} - x_{R,2}(t)}{x_{\Psi,1} - x_{R,1}(t)} \right) \quad (18)$$

where $x = [x_R, x_3]^T$ such that $x_R = [x_{R,1}, x_{R,2}]^T$ is the global position (two coordinates) of the mobile robot and $x_3 \in [0, 2\pi)$ is the robot heading angle; x_G is the coordinate pair of the goal; \bar{V} is a robot constant speed equal to 1; r is 0.5; $x_\Phi = [0, 4]^T$ is the coordinates of obstacle 1; and $x_\Psi = [6, 6]^T$ is the coordinates of obstacle 2.

The control problem given is to select the G2G, Avoid1, or Avoid2 that minimizes

$$J(x(t), x_G(t), t) = \int_t^{t_f} \left\{ \rho \|x_R(t) - x_G(t)\|^2 + \alpha_1 \exp \left(-\frac{\|x_R(t) - x_\Phi\|^2}{\beta_1} \right) + \alpha_2 \exp \left(-\frac{\|x_R(t) - x_\Psi\|^2}{\beta_2} \right) \right\} dt \quad (19)$$

subject to the system equations from the current time t to the end of the simulation t_f . The cost function constants are $\rho = 0.1$, $\alpha_1 = \alpha_2 = 500$, and $\beta_1 = \beta_2 = 0.8$. The goal coordinates are not known *a priori*, rather an

estimate, \tilde{x}_G at $s \geq t$ is used in the cost function:

$$\tilde{x}_G(s, t, x_G(t)) := x_G(t) + \dot{x}_G(t)(s - t) \quad (20)$$

where the derivative of $x_G(t)$ is approximated with $(x_G(t) - x_G(t - t_s))/t_s$. The problem is defined as having $t_0 = 0$, $t_f = 18$, and a sample time, t_s , of 0.1.

Wardi et al. [4] solve the control problem by finding the switching times for a pre-determined mode sequence. During a simulation, a gradient-descent technique is used to regularly update the mode switching times for upcoming modes left in the sequence. Their results are reported further on.

MPP, MIP/MPT, and CPLEX are not suitable for problems having nonlinear dynamics and constraints and/or PIs not linear or not quadratic as in this example of mobile robot tracking and avoidance. The embedding approach has no such limitations. Hence only the embedding approach is used for comparison with the published results in [4].

The three modes carry over to the embedded model and are controlled by \tilde{v}_0 , \tilde{v}_1 , and \tilde{v}_2 :

$$\dot{\tilde{x}}(t) = \tilde{v}_0(t) \begin{bmatrix} V \cos(\tilde{x}_3(t)) \\ V \sin(\tilde{x}_3(t)) \\ u_{G2G} - \tilde{x}_3(t) \end{bmatrix} + \tilde{v}_1(t) \begin{bmatrix} V \cos(\tilde{x}_3(t)) \\ V \sin(\tilde{x}_3(t)) \\ u_{Avoid1} - \tilde{x}_3(t) \end{bmatrix} + \tilde{v}_2(t) \begin{bmatrix} V \cos(\tilde{x}_3(t)) \\ V \sin(\tilde{x}_3(t)) \\ u_{Avoid2} - \tilde{x}_3(t) \end{bmatrix} \quad (21)$$

where $\tilde{v}_i \in [0, 1]$ and $\tilde{v}_0 + \tilde{v}_1 + \tilde{v}_2 = 1$. The embedded control problem is to also minimize (19) over the \tilde{v}_i subject to (21) and the summation constraint on \tilde{v}_i . MATLAB's *fmincon* function is used to solve the problem after converting the continuous-time equations to discrete-time equality constraints via collocation [9]. The cost function is approximated with trapezoidal numerical integration (see Appendix A for more detail).

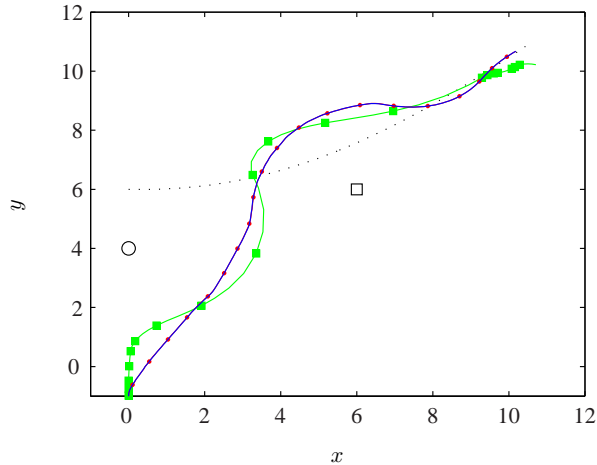


Fig. 3. Mobile robot trajectory over the simulation: (—) EOC with projection, (●) EOC no projection, (■) Wardi et al. off-line solution [4], (·) target path, (○) obstacle 1, (□) obstacle 2.

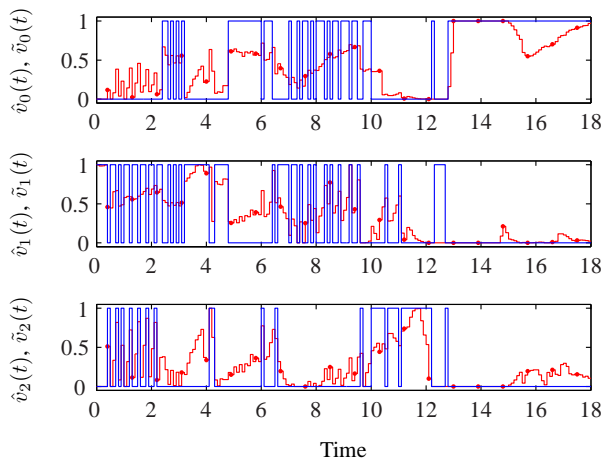


Fig. 4. Mobile robot embedded optimal control mode selection: (—) projected, (●) embedded solution.

A continuation approach [29] is used to construct an initial guess; furthermore, the continuation approach itself is initialized using Appendix A-Step 4. When needed, mode projection is accomplished by selecting the embedded mode switch with the largest value as was done in [23].

Fig. 3 shows the robot trajectories obtained with the embedding approach and using the switching times and

mode selection given in [4] for the off-line solution. Fig. 4 shows computed values for the embedding approach and final projected mode switch values. Mode projection is required approximately 87% of the time. In Wardi et al., the mode sequence is predefined as $\{G2G, \text{Avoid1}, G2G, \text{Avoid2}, G2G\}$ and only the switching times are to be found. The embedding approach makes no such assumptions on the mode selection. The cost obtained with the Wardi et al. offline solution is 22.84 while the embedding approach here results in a simulation cost of 18.83, a reduction of nearly 18%. As a follow-on test, an MPC approach was implemented with a prediction horizon of 1 time unit (10 partitions of 0.1 time units). The MPC optimization and implementation resulted in a simulation cost of 20.56, which is still about 10% less than the offline solution cost of 22.84, and 154 mode projections (out of 180 partitions).

C. Two-Tank Hybrid System [5]

The two-tank hybrid system in [5] consists of the draining of one tank into another with the flow rate into the first tank regulated by a valve with two possible values, $\nu = 1$ and $\nu = 2$. The dynamics are given as

$$\dot{x}(t) = \begin{bmatrix} \nu(t) - \sqrt{x_1(t)} \\ \sqrt{x_1(t)} - \sqrt{x_2(t)} \end{bmatrix} \quad (22)$$

where $x = [x_1, x_2]^T$ with x_1 the level of tank 1 and x_2 the level of tank 2. The initial conditions are $x_1(0) = x_2(0) = 2$ and the states satisfy $x_1, x_2 \in [1, 4]$. The control problem is to select the $\nu(t)$ that minimizes

$$J(x(0), t_f) = 2 \int_0^{t_f} (x_2(t) - 3)^2 dt \quad (23)$$

with $t_f = 20$ and subject to (22) and the state bounds. The sample interval is $t_s = 0.01$ and the continuous-time dynamics are discretized with the forward-Euler method. Wardi and Egerstedt [5] use a gradient-descent technique to solve the control problem like that used for

the mobile robot described previously except the need to predefine the mode sequence is removed. The mode sequence and switch times are calculated to minimize the cost function over the entire simulation time, i.e, it is a global minimum solution approach. The approach relies on an insertion gradient that indicates whether a change in the mode sequence and/or switch times decreases a cost function. The insertion gradient is iteratively driven toward zero over mode sequences and switch times selected according to the solution algorithm.

The two-tank problem is solved using the embedding approach. The MPP, MIP/MPT, or CPLEX methods are not applied to the two-tank problem because of their inability to handle models with square-root terms. The embedded model representation of the two mode two-tank dynamics is

$$\begin{aligned} \dot{\hat{x}}(t) = & (1 - \tilde{v}(t)) \begin{bmatrix} 1 - \sqrt{\tilde{x}_1(t)} \\ \sqrt{\tilde{x}_1(t)} - \sqrt{\tilde{x}_2(t)} \end{bmatrix} \\ & + \tilde{v}(t) \begin{bmatrix} 2 - \sqrt{\tilde{x}_1(t)} \\ \sqrt{\tilde{x}_1(t)} - \sqrt{\tilde{x}_2(t)} \end{bmatrix} \end{aligned} \quad (24)$$

where $\tilde{v} \in [0, 1]$. Notice that the embedded problem does not include continuous control inputs, only the mode needs to be selected. The embedded control problem is to minimize (23) over \tilde{v} subject to (24) and the bounds on the states listed previously. Appendix A outlines how MATLAB's *fmincon* function is used to solve the problem after converting the continuous-time equations to discrete-time equality constraints via the forward-Euler method and approximating the cost function with trapezoidal numerical integration. Mode projection is of the duty cycle type here. For $(1 - \tilde{v})t_{s,E}$, mode 0 with $\nu = 1$ is applied and then for the remainder of the sample interval mode 1 with $\nu = 2$ is used; $t_{s,E}$ is the embedded problem sample interval.

Fig. 5 shows the embedding approach performance for

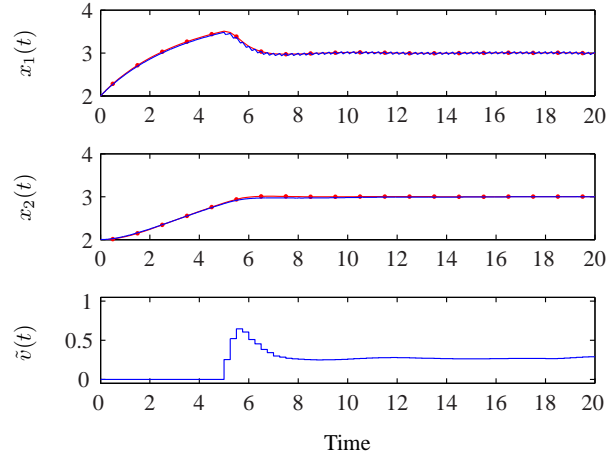


Fig. 5. Two-tank hybrid system example states and embedded mode switch values: (—) EOC with duty cycle mode projection, (•) embedded solution.

$t_{s,E} = 0.25$. The x_2 state reaches the desired value of 3 about 6 time units into the simulation and does not vary more than 1.5% thereafter. In contrast, in [5] the state x_2 shows variation up to about 7% from 6 time units onward and both states show signs of instability as t approaches t_f . The reported cost is 4.78 (recall $t_s = 0.01$). On the other hand, for a time step of 0.25, the embedding approach gives a lower (simulated plant) cost of 4.74 and shows no signs of instability.

D. DC-DC Boost Converter Hybrid System [17]

The DC-DC boost converter model is a switched lumped parameter circuit described in [17]. The boost converter continuous-time dynamics on the time interval $[kt_s, (k+1)t_s]$ are given as

$$\dot{x}(t) = \begin{cases} F_1 x(t) + f_1 v_s, & kt_s \leq t \leq (k + d(k))t_s \\ F_2 x(t) + f_2 v_s, & (k + d(k))t_s < t \leq (k + 1)t_s \end{cases} \quad (25)$$

with

$$F_1 = H_1 \begin{bmatrix} -\frac{r_l}{L} & 0 \\ 0 & -\frac{1}{C(r_o + r_c)} \end{bmatrix} H_1^{-1} \quad (26)$$

$$f_1 = H_1 \begin{bmatrix} \frac{1}{L} & 0 \end{bmatrix}^T \quad (27)$$

$$H_1 = \begin{bmatrix} 1 & 0 \\ 0 & \frac{r_o}{r_o+r_c} \end{bmatrix} \quad (28)$$

$$F_2 = H_2 \begin{bmatrix} -\frac{1}{L} \left(r_l + \frac{r_o r_c}{r_o+r_c} \right) & -\frac{r_o}{L(r_o+r_c)} \\ \frac{r_o}{C(r_o+r_c)} & -\frac{1}{C(r_o+r_c)} \end{bmatrix} H_2^{-1} \quad (29)$$

$$f_2 = H_2 \begin{bmatrix} \frac{1}{L} & 0 \end{bmatrix}^T \quad (30)$$

$$H_2 = \begin{bmatrix} 1 & 0 \\ \frac{r_o r_c}{r_o+r_c} & \frac{r_o}{r_o+r_c} \end{bmatrix} \quad (31)$$

where $x = [i_l, v_o]^T$, i_l is the inductor current, v_o is the output voltage, v_s is the supply voltage, and $d \in [0, 0.95]$ is the duty cycle in the interval. The model parameters are $C = 100 \mu\text{F}$, $L = 2 \text{ mH}$, $r_c = 0.1 \Omega$, $r_l = 0.5 \Omega$, $r_o = 200 \Omega$, and the maximum inductor current is 2.5 A ; the switching frequency is 20 kHz (the sample interval, t_s , is $50 \mu\text{s}$).

For MPP control in [17], (25) is not used in the actual optimization. Rather, linearized, discrete-time models developed from (25) corresponding to one of three regions of the duty cycle interval, $D_0 = [0.0, 0.45]$, $D_1 = [0.45, 0.6]$, and $D_2 = [0.6, 0.95]$, are used:

$$x'(k+1) = A_{m,i} x'(k) + B_{m,i} d(k) + f_{m,i}, \quad (32)$$

where $x'(t) = [i'_l, v'_o]^T = [i_l/v_s, v_o/v_s]^T$ (the original state is divided by v_s to avoid the need to generate new linear models if v_s changes) and $i = 0, 1, 2$ designates the duty cycle region of the model. Appendix B describes the process of generating the linear model in [17] and lists the $A_{m,i}$, $B_{m,i}$, and $f_{m,i}$ found.

The MPP control performance index given in [17] for a horizon window of length N is

$$J(x(k), D_k, N) = \sum_{k=0}^{N-1} \|Q(v'_o(k+l|k) - v'_{o,ref}(k))\|_p^q + \|R(d(k+l|k) - d(k+l-1|k))\|_p^q \quad (33)$$

where $D_k = [d(k-1), \dots, d(k+N-1)]$, Q and R are penalty weight scalars, $v'_{o,ref}(k) = v_{o,ref}/v_s$ is a given reference output voltage (assumed constant over N), and p designates the norm. The problem parameters given are $x(0) = [0, v_s]^T$, $N = 18$, $v_{o,ref} = 50 \text{ V}$, $v_s = 25 \text{ V}$, $Q = 10$, $R = 1$, $p = 1$, and $q = 1$. The application of the duty cycle to the plant is given as being delayed by one sample time interval. In [17], the duty cycle is fixed to the same value over the N partition prediction horizon, reducing the optimization to a simple one-dimensional search rather than an N -dimensional search as would be consistent with a normal MPC framework.

The MPP, MIP/MPT, and embedding approach are compared using a 1-norm PI as in the original problem; CPLEX and the embedding approach are compared using a squared 2-norm (quadratic) PI because CPLEX is not able to calculate a p-norm PI. Also, the limiting assumption of a fixed duty cycle over the prediction horizon is removed. Furthermore, the embedding approach theory is not yet developed for p-norm weights on the embedded switch values, i.e., the duty cycle values as seen later, thus R is set to zero in the subsequent HOCP solution approaches.

The MPP, MIP/MPT, CPLEX and the embedding approach algorithm specific boost converter HOCP formulations are now set forth. To apply MPP and MIP/MPT control using the MPT, $x'(k)$ is augmented with $d(k-1)$ and $v'_{o,ref}$ states to form a new state vector $x''(k) = [i'_l(k), v'_o(k), d(k-1), v'_{o,ref}(k)]^T$; the control input is $\Delta d(k)$. The equivalent performance index to (33) is

$$J(x''(k), \Delta D_k, N) = \sum_{l=0}^{N-1} \|Q' x''(k+l|k)\|_1 + \|R \Delta D_k\|_1 \quad (34)$$

where $\Delta D_k = [\Delta d(k), \dots, \Delta d(k+N-1)]^T$, $R = 0$, and $Q'(2, 2) = 10$ and $Q'(2, 4) = -10$.

CPLEX is the next solution approach to the boost

converter HOCP presented. CPLEX is not able to solve problems with p-norm performance indices therefore the quadratic PI is (33) with $p = 2$ and $q = 2$. Also, the boost converter dynamics are modeled in CPLEX using (32), developed for the MPP and MIP/MPT control, because CPLEX accepts only linear equality constraints.

The embedding approach is now considered for the boost converter HCOP. Unlike for MPP and MIP (MIP/MPT and CPLEX), the true boost converter dynamics, (25), are used in the optimization; there is no need for ad hoc pseudo-model generation. The boost converter dynamics in the embedded model formulation are

$$\begin{aligned} \dot{\tilde{x}}(t) = & (1 - \tilde{v}(t))(F_2\tilde{x}(t) + f_2v_s) \\ & + \tilde{v}(t)(F_1\tilde{x}(t) + f_1v_s) \end{aligned} \quad (35)$$

The embedded optimal control problem is to minimize

$$J_E(x(t_0^p), \tilde{v}, t_0^p, t_f^p) = \int_{t_0^p}^{t_f^p} \|Q_E(\tilde{v}_o(t) - v_{o,ref}(t))\|_p^q dt \quad (36)$$

over $\tilde{v} \in [0, 1]$ subject to (35). Q_E , p , and q are chosen such that the trapezoidal numerical integration approximation of (36) is consistent with the PI of the MPP, MIP/MPT, or CPLEX approach being compared. The EOCP is solved using MATLAB's *fmincon* function after converting the continuous-time dynamic equations to discrete-time equality constraints via collocation and approximating the cost function with trapezoidal numerical integration (see Appendix A for the solution method outline). Mode projection of an optimal \tilde{v} consists of using it directly as a duty cycle, d over a partition.

The comparisons of the boost converter HOCP solution methods is carried out using $N = 4$, $N = 6$, and $N = 12$ and reference output voltage of

$$v_{o,ref}(t) = \begin{cases} 35 \text{ V}, & 25 \text{ ms} \leq t \leq 35 \text{ ms} \\ 50 \text{ V}, & \text{otherwise.} \end{cases} \quad (37)$$

TABLE II
DC-DC BOOST CONVERTER EXAMPLE EOC (DUTY CYCLE INTERPRETATION), MPP, AND MIP/MPT 1-NORM PERFORMANCE INDEX COST J , AND SOLUTION TIMES, Δt^r , FOR THE SIMULATION. (X IS NO DATA.)

Metric	$N = 4$	$N = 6$	$N = 12$
J_E	917.33	818.45	808.94
J_{MPP}	5651.93	X	X
$J_{MIP/MPT}$	970.09	954.95	X
Δt_E^r (s)	85.17	804.50	3789.53
Δt_{MPP}^r (s)	2630.98	X	X
$\Delta t_{MIP/MPT}^r$ (s)	103.87	1145.07	X

TABLE III
DC-DC BOOST CONVERTER EXAMPLE EOC (DUTY CYCLE INTERPRETATION) AND CPLEX SQUARED 2-NORM PERFORMANCE INDEX COST WITH (36), J , AND SOLUTION TIMES, Δt^r , FOR THE SIMULATION.

Metric	$N = 4$	$N = 6$	$N = 12$
J_E	12593.16	9969.59	9291.08
J_{CPLEX}	156547.91	11512.15	10297.26
Δt_E^r (s)	50.79	81.82	267.17
Δt_{CPLEX}^r (s)	96.06	129.56	31605.55

Longer prediction horizons, like $N = 18$, are not considered since it has been shown that longer prediction horizons do not provide significantly better control [30]. Table II lists the MPP, MIP/MPT, and embedding approach 1-norm PI costs and total control solution times. In all tests, the embedding approach provided the least cost and fastest solution time when a comparison could be made to MPP and MIP/MPT. In several instances, MPP and MIP/MPT solutions are not listed because control solutions were not generated after 40 hours and the test was stopped. Table III shows the CPLEX and embedding approach quadratic PI costs and total control solution times. The embedding approach costs are lower

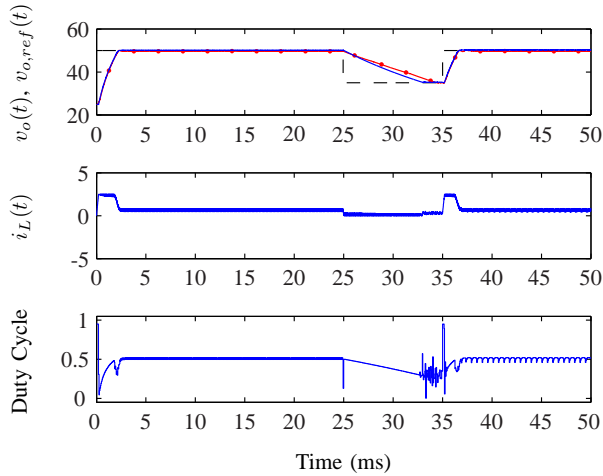


Fig. 6. Boost converter hybrid system states and duty cycle from embedding solution approach with $N = 12$: (—) EOC with duty cycle mode projection, (•) CPLEX, (---) $v_{o,ref}$.

than the CPLEX costs in each test. Also, as N is increased the cost decreases for both solution methods. The embedding approach solution time for $N = 4$, $N = 6$, and $N = 12$ are about 2, 1.6, and 120 times faster than the CPLEX times, respectively. The fact that the CPLEX solution time dramatically increases over the embedding approach time when $N = 12$ illustrates the “curse of dimensionality” associated with mixed-integer programming. Boost converter control using the embedding approach implemented in a dedicated micro-controller has been solved as fast as $50 \mu\text{s}$ [13].

Fig. 6 shows embedding and CPLEX approach results for $N = 12$. The (37) reference output voltage appears to be better tracked with the embedding approach during the step change in $v_{o,ref}$ to 35 V on [25, 35] ms. The embedding approach is better able to track the 50 V reference on [10, 25] ms (after the initial voltage rise and before the step change in v_o) than CPLEX; the average v_o on [10, 25] ms from the embedding approach is 50.15 V while that from CPLEX is 49.69 V, the error with the embedding approach is about half that

of CPLEX.

One final point, good control performance requires an accurate value of the possibly varying load resistance and good estimates of the resistance have been achieved using a nonlinear resistance error system [16]. MPP, MIP/MPT, nor CPLEX has the capability to incorporate a nonlinear estimator directly into the control problem like the embedding approach.

E. Skid-Steered Vehicle Hybrid System [18], [19]

A skid-steered vehicle (SSV) movement hybrid problem is set forth by Caldwell and Murphey in [18], [19]. They identify four modes of operation during SSV movement depending on the lateral sticking or sliding of the wheels: mode 1, front and rear wheels sticking laterally; mode 2, front wheels sticking laterally and back wheels skidding laterally; mode 3, front wheels skidding laterally and back wheels sticking laterally; and mode 4, front and rear wheels skidding laterally. The equations of motion for modes 1 and 4 are given in [19]¹; mode 2 and 3 dynamics are listed in Appendix C due to their length.

$$f_1 := \begin{cases} \ddot{X}(t) = \frac{(F_1 + F_2 + F_3 + F_4) \cos \theta(t)}{M} - c_1 \dot{X}(t) \\ \dot{Y}(t) = \frac{(F_1 + F_2 + F_3 + F_4) \sin \theta(t)}{M} - c_1 \dot{Y}(t) \\ \ddot{\theta} = 0 \end{cases}$$

(38)

¹The sign on the $\dot{\theta}$ term in mode 4 is negative here rather than positive as in [19] and was changed after correspondence with the authors.

$$f_4 := \begin{cases} \ddot{X}(t) = \frac{(F_1+F_2+F_3+F_4) \cos \theta(t)}{M} - c_4 \dot{X}(t) \\ \quad + \mu_k g \sin \theta(t) [-\dot{X}(t) \sin \theta(t) + \dot{Y}(t) \cos \theta(t)] \\ \ddot{Y}(t) = \frac{(F_1+F_2+F_3+F_4) \sin \theta(t)}{M} - c_4 \dot{Y}(t) \\ \quad - \mu_k g \cos \theta(t) [-\dot{X}(t) \sin \theta(t) + \dot{Y}(t) \cos \theta(t)] \\ \ddot{\theta}(t) = \frac{b(F_1-F_2-F_3+F_4) - a^2 \mu_K M g \dot{\theta}(t)}{J} \end{cases} \quad (39)$$

with

$$M = m_b + 4m_w \quad (40)$$

$$J = 4m_w(a^2 + b^2) + \frac{4m_w}{12}(w_w^2 + 3w_r^2) + \frac{m_b}{12}(B_l^2 + B_w^2) \quad (41)$$

where X , Y , and θ are position and orientation coordinates in the global coordinate frame; F_1/F_2 is the right/left rear wheel torque; F_4/F_3 is the right/left front wheel torque; c_i are mode specific damping coefficients; μ_K is the coefficient of kinetic friction; m_b is the body mass; m_w is a wheel mass; B_l/B_w is the SSV body length/width; a/b is half the distance from wheel center to wheel center in the vehicle length/width direction; w_w is half the wheel width; and w_r is the wheel radius. Model parameters from [18], [19]² are $c_1 = 0.7$, $c_2, c_3, c_4 = 1.2$, $\mu_K = 0.8$, $m_b = 70$ kg, $m_w = 2.5$ kg, $B_l = 0.8$ m, $B_w = 0.6$ m, $a = 0.16$ m, $b = 0.28$ m, and $w_w, w_r = 0.14$ m.

Caldwell and Murphey use the SSV mode-dependent model to first generate the vehicle response given wheel torques (shown in Figure 3 in [19]) and mode values over a 15 s period. The mode sequence is (1, 4, 1) with switchings occurring at 5 s and 11 s. Next, the simulation output is used as reference values to be tracked in a HOCP in an effort to try to recover the simulation mode

²Values for c_2 , c_3 , w_w , and w_r were obtained through personal correspondence with Caldwell and Murphey.

switches. The SSV HOCP is to minimize the following cost [19]:

$$J(\tilde{v}) = 0.5(\tilde{x}(t_f) - x_{ref}(t_f))^T P(\tilde{x}(t_f) - x_{ref}(t_f)) + \int_{t_0}^{t_f} 0.5(\tilde{x}(t) - x_{ref}(t))^T Q(\tilde{x}(t) - x_{ref}(t)) dt \quad (42)$$

subject to a relaxed switched system representation of the dynamics, i.e., an embedded representation:

$$\dot{\tilde{x}}(t) = \sum_{i=1}^4 \tilde{v}_i f_i(\tilde{x}) \quad (43)$$

$$\sum_{i=1}^4 \tilde{v}_i = 1 \quad (44)$$

where $\tilde{x} = [\tilde{X}, \dot{\tilde{X}}, \tilde{Y}, \dot{\tilde{Y}}, \tilde{\theta}, \dot{\tilde{\theta}}]^T$, $Q = \text{diag}(1, 1, 1, 1, 1, 1)$, $P = \text{diag}(1, 10, 1, 10, 1, 10)$, $t_0 = 0$ s, and $t_f = 15$ s. Finally, the active mode is chosen as the mode associated with the greatest value of \tilde{v}_i . This is the mode projection method in Meyer et al. [23] found to give the least cost in an empirical study of projection methods applied to an example hybrid optimal control problem solved with embedding. Caldwell and Murphey [19] showed that the embedding approach and mode projection can recover switched system modes for the SSV described here. Their approach was presented as a heuristic development independent of the work in [8]. In contrast, [8] provides a theoretically rigorous justification of the embedding approach and shows that it essentially always leads to a solution of the SOCP.

The embedded problem is solved here and the mode projection method used in Caldwell and Murphey is applied. Again, due to the nonlinear nature of the problem, MPP, MIP/MPT, and CPLEX methods cannot be utilized. For the embedded problem, the 15 s simulation time is divided into 60 equal length partitions. The HOCP embedding approach solution follows Appendix A where the continuous-time cost integration is represented with trapezoidal numerical integration and

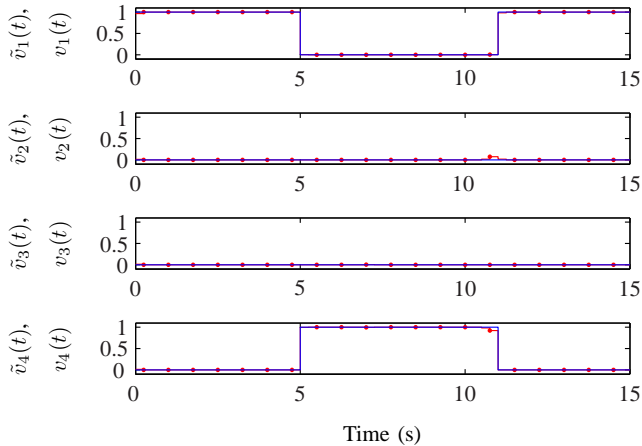


Fig. 7. Skid-steered vehicle embedded solution and projected modes: (—) embedded, (•) projected.

embedded continuous-time dynamics are transformed into equality constraints using collocation. The original mode sequence and switching times used to generate the reference state trajectories is recovered using embedding and projection as shown in Fig. 7; mode projection was required for 10% of the partitions. Also, the embedded solution cost is $2.1 \cdot 10^{-4}$, meaning the embedded solution tracked the reference trajectories well.

F. 11 State-Space Region Autonomous Switch Example [6]

Passenberg et al. [6], [7] proposed a version of a hybrid system minimum principle and applied it to an 11 a-mode linear system. In the example, a state space, \mathbb{R}^2 , is divided into 11 polygonal regions, each associated with a distinct linear state dynamic. Thus, a discrete state $q(t) \in \{1, 2, \dots, 11\}$ identifies a continuous-time state dynamic:

$$\dot{x}(t) = A_q x(t) + B_q u(t) \quad (45)$$

where $x \in \mathbb{R}^2$, $u \in U_q \subset \mathbb{R}^2$, $A_q \in \mathbb{R}^{2 \times 2}$ constant, and $B_q \in \mathbb{R}^{2 \times 2}$ constant. The 11 regions are illustrated in

Fig. 8. Each region also has an associated PI integrand:

$$F_q(x, u) = 0.5x^T(t)S_q x(t) + 0.5u^T(t)R_q u(t) \quad (46)$$

where $S_q, R_q \in \mathbb{R}^{2 \times 2}$ are constant penalty weight matrices that depend on q . Given a system trajectory $(x(t), u(t))$, the associated discrete state sequence $\{q_1, \dots, q_K\}$ and the switching time sequence $\{t_0, \dots, t_K\}$ (t_0 and t_K are the initial and final time, respectively), such that $x(t)$ belongs to region q_j if $t_{j-1} < t < t_j$, the PI is then:

$$J(x(t), u(t)) = \sum_{k=1}^K \int_{t_{k-1}}^{t_k} F_{q_k} dt. \quad (47)$$

The optimal control problem is to drive the states from $x(t_0) = [-8, -8]^T$ at $t_0 = 0$ to the origin at $t_K = 2$ such that the PI in (47) is minimized subject to (45) and constraints on u due to U_q (which is not the same for all values of q). The A_q , B_q , S_q , R_q , and U_q are listed in Appendix D along with the state-space partition boundary equations. In this 11 state-space regions problem, all the switches are autonomous. At the switching surfaces both the vector fields and the performance index are nonsmooth, which is problematic for traditional optimization methods such as SQP.

The optimization algorithm in [7] can be summarized as follows:

- 1) Choose a feasible sequence of discrete states (adjacent regions) and an appropriate number of switching points (switching time and the value of the state at the switch) on the switching manifolds.
- 2) Find the optimal value for the continuous control $u(t)$ by solving a set of traditional optimization problems for which the switching points provide the fixed initial and final states and times.
- 3) Determine the gradient of the PI at the (autonomous) switching points.

- 4) Based on the gradient computed in Step 3 and the local geometry of the switching manifolds around the switching point, determine the next sequence of the discrete states (regions) and switching points.
- 5) Stop if the next switching points are within a certain tolerance of the current ones otherwise return to Step 2.

In our view, Step 4 is the critical step and the main insight of Passenberg et al. In particular, by separating the computation of the continuous controls from the computation of the switching points, the nonsmoothness at the switching points is completely avoided. Passenberg et al. [6] reported a solution cost of 14.69 for the example with 172 nonuniform time partitions; the solution trajectory is shown in Fig. 8³.

In our previous work [9], [21] we showed that problems involving a-modes, i.e., autonomous switches, can be solved using traditional mathematical programming methods (in particular, SQP) without any special consideration of the switches and the nonsmoothness associated with them. However, if applied to the example above, the direct application of SQP results in a slightly suboptimal solution.

To evaluate our approach, we first applied traditional numerical programming as suggested in [9] with 172 uniform length partitions; for better numerical solution behavior, B_q and R_q were scaled so that the continuous controls, u , lie in $[-1, 1] \times [-1, 1]$ for each q . Since all switches are autonomous, no embedding in the vein of [21] is necessary. Starting from an initial guess obtained using continuation [29] (which is initialized using Step 4 in Appendix A), we obtained a numerical optimization cost of 14.71 and simulated plant cost with

³Passenberg supplied their trajectories in [6] for Fig. 8 through personal correspondence.

TABLE IV
11-REGION AUTONOMOUS SWITCHED SYSTEM PROBLEM COST FOR
PASSENBERG ET AL., TRADITIONAL NUMERICAL PROGRAMMING
(TNP), AND TNP WITH SWITCHING POINT TIME ITERATION
(TNP/ITER).

Optimization	Reported Cost	
Passenberg et al. [6]	14.69	
Optimization	Optimization Solution Cost	Simulation Cost
TNP	14.71	14.81
TNP/iter	14.69	14.71

the computed piecewise continuous controls of 14.81, slightly larger than the Passenberg et al. cost of 14.69.

This solution can be improved by accounting for the (discontinuous) transitions across the switching manifolds. To explicitly account for region transitions, we identified the time partitions in which they occur, estimated the crossover times, appropriately subdivided each identified partition into two of unequal lengths, and then re-optimized. This resulted in a numerical programming cost of 14.69 and simulation cost of 14.71 after 10 iterations on the estimated crossover times, which is consistent with Passenberg et al. reported cost. As an alternative, once the sequence of the discrete states is computed, methods that solve the hybrid optimal control problem assuming a known sequence of discrete states [4], [25], [31] can be used to compute the optimal switching points.

Table IV lists the (similar) costs reported from Passenberg et al. and those obtained here. The trajectory given by Passenberg et al. and the one obtained in the research reported herein using 172 uniform time partitions are plotted in Fig. 8; one observes the closeness of the trajectories computed by each of the two algorithms, Passenberg et al. and ours. The authors would like to

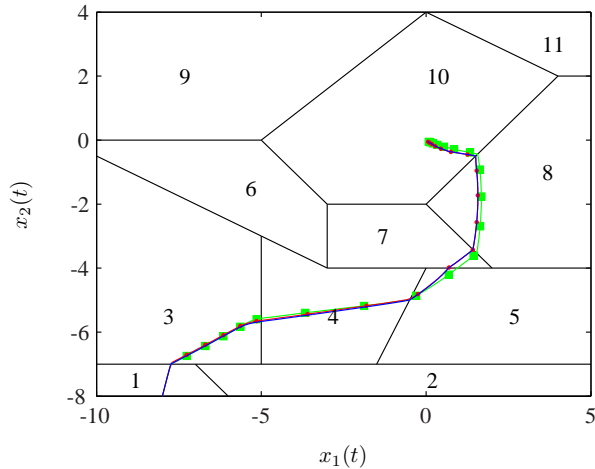


Fig. 8. Autonomous switched system with 11 a-modes state path through the labeled state-space partitions: (—) simulation, (•) states from traditional numerical programming solution with 172 uniform time partitions, (■) Passenberg et al. solution [6].

acknowledge that the algorithm of Passenberg et al. has an advantage due to the explicit handling of the switching- or discontinuity-manifolds. In order for classical optimization such as SQP (as asserted in [9]) to obtain similar results, transitions across discontinuity manifolds must be properly accounted for. Please note MPP, MIP/MPT, and CPLEX are not applied to this problem because they do not allow for switched PI penalty weights.

III. DISCUSSION

The six hybrid optimal control problem examples presented demonstrate the differences and similarities between the embedding approach, MPP, MIP (MIP/MPT and CPLEX), and gradient based methods as well as the applicability of traditional numerical programming to autonomously switched systems. Table V lists key differences between the various HOCP solution approaches. From the table, the embedding approach addresses a wider class of problems, does not require a specialized solver to implement, does not require additional variables

for autonomous switches, and does not require supplying an initial mode sequence. Furthermore, the previous examples showed that the embedding approach led to a solution in all cases, the embedding approach solutions costs were less than or equal to the other methods costs (when available), and the embedding approach problem was solved in less time (when available) than the other methods except for CPLEX. CPLEX’s specialized routines resulted in solution times an average of one-third that of the embedding approach in the spring-mass example. The embedding approach utilizes MATLAB’s *fmincon* general purpose optimizer and is not streamlined for a specific class of problems like CPLEX. However, in the DC-DC boost converter example CPLEX took about 120 times longer than the embedding approach to solve the 12 partition control and prediction horizon boost converter problem, illustrating the “curse of dimensionality” associated with mixed-integer programming. The embedding approach solution can be implemented in real-time as illustrated in [13] where a boost converter problem is solvable in about $50 \mu\text{s}$ using a specialized algorithm.

IV. CONCLUSION

This paper delineates specific differences between the embedding approach for solving hybrid optimal control problems and multi-parametric programming, mixed-integer programming, and gradient-descent based methods. First, the embedding approach’s theoretical underpinnings guarantee the existence of a solution under mild conditions. Second, the embedding approach generates a convex problem and is solvable with widely available optimization packages such as sequential quadratic programming. Third, the embedding approach permits nonlinear state models as long as they are linear in the continuous time controls. Fourth, the embedding

TABLE V
HYBRID OPTIMAL CONTROL PROBLEM SOLUTION APPROACHES KEY DIFFERENCES (GDB IS GRADIENT DESCENT BASED METHODS).

Characteristic	Embedded	MPP	MIP/MPT	CPLEX	GDB [4]/[5]
General nonlinear control models allowed	Yes	No	No	No	Yes/Yes
Switched PI weights allowed	Yes	No	No	No	No/No
Utilizes traditional numerical programming	Yes	No	No	No	No/No
Computational complexity is NP-hard and rises exponentially with no. of modes	No	Yes	Yes	Yes	No/No
Autonomous switches need discrete states assigned	No	Yes	Yes	Yes	-/-
Problem initialized with predefined mode sequence	No	No	No	No	Yes/No
Real time control Implementation	Yes	No	No	No	No/No

approach does not require any assumptions about the mode sequence.

The embedding approach was applied to five hybrid control examples in the literature and results compared to the multi-parametric programming, mixed-integer programming, or gradient-descent method. The embedding approach produced equal to or lower performance index costs and faster online solution times than the other optimization methods with the exception of CPLEX in the spring-mass example. We attribute this to the specialized nature of the CPLEX solver as compared to the general MATLAB solver used to solve the embedded problem. Also, the embedding approach found control solutions when other methods failed. In the sixth hybrid control example, an 11 autonomous-mode switched system which did not require embedding, we found the solution cost obtained with a hybrid minimum principle to be slightly less than that using traditional numerical programming; the important insight is that the numerical algorithm must account for discontinuities in the vector fields either implicitly or explicitly as is done in [6], [7]. In summary, the embedding approach offers less problem set up and outstanding numerical results.

APPENDIX A

APPENDIX: MATLAB EMBEDDING SOLUTION APPROACH ALGORITHM

Here we outline the steps to solve a hybrid optimal control problem with the embedding approach using MATLAB's *fmincon* function.

- 1) (For continuous-time optimal control problem.) Transform the continuous-time embedded system dynamics into discrete time using the lengths of the prediction horizon partitions and either the forward-Euler, backward-Euler, or direct collocation with triangular basis functions [9] methods. The resulting discretized embedded optimal control problem dynamics are a series of nonlinear equalities.
- 2) (For continuous-time optimal control problem.) Discretize the PI cost over the prediction horizon partitions using trapezoidal numerical integration.
- 3) Create equality constraints that enforce any supervisory-level interconnections and embedded mode value sum (embedded mode switch values sum to one) at the midpoint of each MPC partition if the problem was originally formulated in continuous time or partition boundary if the problem was given indiscrete time.
- 4) Obtain an initial guess for the *fmincon* variables

to be solved for: states, algebraic variables, control inputs, and modes. The initial guess comes from the immediately previous EOCP solution, i.e., a warm start [32], when $t_0^p > t_0$. For the first EOCP solution, $t_0^p = t_0$, an in-house created pre-processing function is used to find the initial guess. This function works by first solving the EOCP (to a lower numerical tolerance than normal, $1 \cdot 10^{-3}$ versus $1 \cdot 10^{-6}$) using *fmincon* for one partition ahead with a user specified initial guess. Then, partitions are successively added to the problem, with the EOCP solved after each addition, until the prediction horizon is reached. During partition addition, the solution associated with the previously added partition is carried forward to populate the initial guess of the current EOCP problem.

- 5) Solve the EOCP using *fmincon*.
- 6) Perform any mode and control projection on the controls for the first partition of the prediction horizon if the partition's EOCP solution is singular with some mode switch values in $(0, 1)$. Theoretically, singular solutions occur when two of the possible mode-dependent Hamiltonians are numerically equal which occurs with small probability, generically, thus making bang-bang type solutions the norm.
- 7) Either obtain a hardware measurement at the end of the current partition or execute a high accuracy simulation of the continuous-time switched system with the computed controls over one partition using MATLAB's *ode23t* function.
- 8) Slide the starting time of the prediction horizon ahead one partition. If the end of the simulation is not reached, return to Step 4.

APPENDIX B

DC-DC BOOST CONVERTER PIECE-WISE DYNAMICS [17]

The linear DC-DC boost converter dynamics for each duty cycle interval were developed using the procedure outlined in [17]. First, the duty cycle is divided into three regions: $D_0 = [0.0, 0.45]$, $D_1 = [0.45, 0.6]$, and $D_2 = [0.6, 0.95]$. Second, the allowable initial state conditions are specified. The scaled inductor current, $i'_l = i_l/v_s$, initial condition is taken to lie in $[0, 0.03]$ A/V while the scaled output voltage, $v'_o = v_o/v_s$, initial condition is on $[0, 1.6]$. Third, the simulation data for a duty cycle interval is generated. The duty cycle, inductor current, and output voltage intervals are discretized using five evenly spaced points, then all possible combinations of the points are simulated over a time interval of t_s duration using (25). Mariehoz et al. [17] do not provide the inductor current or output voltage intervals nor do they give the number of points in the discretization of the intervals. Fourth, the simulation data is fit to (32) using least squares. The resulting linear models associated with the duty cycle intervals are

$$A_{m,0} = \begin{bmatrix} 0.9874 & -0.01426 \\ 0.2835 & 0.9939 \end{bmatrix} \quad (48)$$

$$B_{m,0} = \begin{bmatrix} 0.02828 \\ 0.009680 \end{bmatrix}, \quad f_{m,0} = \begin{bmatrix} 0.01347 \\ 3.736 \cdot 10^{-3} \end{bmatrix}$$

$$A_{m,1} = \begin{bmatrix} 0.9862 & -0.01184 \\ 0.2342 & 0.9949 \end{bmatrix} \quad (49)$$

$$B_{m,1} = \begin{bmatrix} 0.02000 \\ -0.009690 \end{bmatrix}, \quad f_{m,1} = \begin{bmatrix} 0.01431 \\ 0.01074 \end{bmatrix}$$

$$A_{m,2} = \begin{bmatrix} 0.9872 & -5.600 \cdot 10^{-3} \\ 0.1109 & 0.9965 \end{bmatrix} \quad (50)$$

$$B_{m,2} = \begin{bmatrix} 0.01999 \\ -0.01526 \end{bmatrix}, \quad f_{m,2} = \begin{bmatrix} 9.339 \cdot 10^{-4} \\ 0.01477 \end{bmatrix}.$$

APPENDIX C
SKID-STEERED VEHICLE HYBRID SYSTEM
DYNAMICS [19]

Caldwell and Murphey [19] skid-steered vehicle mode 2 (front wheels sticking laterally and back wheels skidding laterally) and 3 (front wheels skidding laterally and back wheels sticking laterally) dynamics⁴ are given next. Mode 2 dynamics, f_2 , are

$$\begin{aligned} \ddot{X}(t) = & \frac{1}{M} \left\{ (F_1 + F_2 + F_3 + F_4) \cos(\theta(t)) \right. \\ & + \frac{\mu_K M g}{2} \sin(\theta(t)) v_{2,y} \\ & + \frac{1}{a} \sin(\theta(t)) [b(F_1 - F_2 - F_3 + F_4) + \frac{\mu_K M g a}{2} v_{2,y}] \\ & - 12J \sin(\theta(t)) [b(F_1 - F_2 - F_3 + F_4) + a^2 \mu_K M g \dot{\theta}(t)] \\ & - aM \dot{X}(t) (\mu_K g \sin(\theta(t)) - \cos(\theta(t)) \dot{\theta}(t)) \\ & \left. + aM \dot{Y}(t) (\mu_K g \cos(\theta(t)) + \sin(\theta(t)) \dot{\theta}(t)) \right\} / (a12K_J) \\ & - c_2 \dot{X}(t) \end{aligned} \quad (51)$$

⁴Caldwell supplied the mode 2 and 3 dynamics through personal correspondence.

$$\begin{aligned} \ddot{Y}(t) = & [\dot{X}(t) + \tan(\theta(t)) \dot{Y}(t)] \dot{\theta}(t) \\ & + \frac{1}{aM} \sin(\theta(t)) \tan(\theta(t)) [b(F_1 - F_2 - F_3 + F_4) \\ & + \frac{a\mu_K M g}{2} v_{2,y}] \\ & - \frac{\tan(\theta(t))}{M} [-(F_1 + F_2 + F_3 + F_4) \cos(\theta(t)) \\ & - \frac{\mu_K M g}{2} \sin(\theta(t)) v_{2,y}] \\ & - \frac{1}{2aM12K_J} \left\{ [12(J + 2a^2M) - 12J \cos(2\theta(t))] \right. \\ & \times \sec(\theta) [b(F_1 - F_2 - F_3 + F_4) + a^2 \mu_K M g \dot{\theta}(t)] \\ & - aM \dot{X}(t) (\mu_K g \sin(\theta(t)) - \cos(\theta(t)) \dot{\theta}(t)) \\ & \left. + aM \dot{Y}(t) (\mu_K g \cos(\theta(t)) + \sin(\theta(t)) \dot{\theta}(t)) \right\} \\ & - c_2 \dot{Y}(t) \end{aligned} \quad (52)$$

$$\begin{aligned} \ddot{\theta}(t) = & -12[b(F_1 - F_2 - F_3 + F_4) + a^2 \mu_K M g \dot{\theta}(t)] \\ & - aM \dot{X}(t) (\mu_K g \sin(\theta(t)) - \cos(\theta(t)) \dot{\theta}(t)) \\ & + aM \dot{Y}(t) (\mu_K g \cos(\theta(t)) + \sin(\theta(t)) \dot{\theta}(t)) / (12K_J) \end{aligned} \quad (53)$$

with

$$M = m_b + 4m_w \quad (54)$$

$$\begin{aligned} J = & 4m_w(a^2 + b^2) + \frac{4m_w}{12}(w_w^2 + 3w_\tau^2) \\ & + \frac{m_b}{12}(B_t^2 + B_w^2) \end{aligned} \quad (55)$$

$$K_J = J + Ma^2 \quad (56)$$

$$v_{2,y} = -\sin(\theta) \dot{X}(t) + \cos(\theta) \dot{Y}(t) + a\dot{\theta}(t). \quad (57)$$

Mode 3 dynamics, f_3 , are

$$\begin{aligned}
\ddot{X}(t) = & \frac{1}{M} \left\{ (F_1 + F_2 + F_3 + F_4) \cos(\theta(t)) \right. \\
& - \frac{\mu_K M g}{2} \sin(\theta(t)) v_{3,y} \\
& - \frac{1}{a} \sin(\theta(t)) [b(F_1 - F_2 - F_3 + F_4) + \frac{a\mu_K M g}{2} v_{3,y}] \\
& + 12J \sin(\theta(t)) [b(F_1 - F_2 - F_3 + F_4) + a^2 \mu_K M g \dot{\theta}(t)] \\
& + aM \dot{X}(t) (\mu_K g \sin(\theta(t)) - \cos(\theta(t)) \dot{\theta}(t)) \\
& \left. - aM \dot{Y}(t) (\mu_K g \cos(\theta(t)) + \sin(\theta(t)) \dot{\theta}(t)) / (a12K_J) \right\} \\
& - c_3 \dot{X}(t)
\end{aligned} \tag{58}$$

$$\begin{aligned}
\ddot{Y}(t) = & [\dot{X}(t) + \tan(\theta(t)) \dot{Y}(t)] \dot{\theta}(t) \\
& - \frac{1}{(aM)} \sin(\theta(t)) \tan(\theta(t)) [b(F_1 - F_2 - F_3 + F_4) \\
& + \frac{a\mu_K M g}{2} v_{3,y}] \\
& - \frac{\tan(\theta(t))}{M} [-(F_1 + F_2 + F_3 + F_4) \cos(\theta(t)) \\
& + \mu_K M g \sin(\theta(t)) v_{3,y}] \\
& + \frac{1}{2aM12K_J} \left\{ [12(J + 2a^2M) - 12J \cos(2\theta(t))] \right. \\
& \times \sec(\theta(t)) [b(F_1 - F_2 - F_3 + F_4) + a^2 \mu_K M g \dot{\theta}(t)] \\
& + aM \dot{X}(t) (\mu_K g \sin(\theta(t)) - \cos(\theta(t)) \dot{\theta}(t)) \\
& \left. - aM \dot{Y}(t) (\mu_K g \cos(\theta(t)) + \sin(\theta(t)) \dot{\theta}(t)) \right\} \\
& - c_3 \dot{Y}(t)
\end{aligned} \tag{59}$$

$$\begin{aligned}
\ddot{\theta}(t) = & -12[b(F_1 - F_2 - F_3 + F_4) + a^2 \mu_K M g \dot{\theta}(t)] \\
& + aM \dot{X}(t) (\mu_K g \sin(\theta(t)) - \cos(\theta(t)) \dot{\theta}(t)) \\
& - aM \dot{Y}(t) (\mu_K g \cos(\theta(t)) + \sin(\theta(t)) \dot{\theta}(t)) / (12K_J)
\end{aligned} \tag{60}$$

with

$$v_{3,y} = \sin(\theta) \dot{X}(t) - \cos(\theta) \dot{Y}(t) + a \dot{\theta}(t). \tag{61}$$

APPENDIX D

11-REGION AUTONOMOUS SWITCH EXAMPLE DYNAMICS AND STATE-SPACE DIVISIONS [6], [7]

Passenberg et al. [6] 11-region autonomous switched system matrices (A_q , B_q), control bounds (U_q), PI matrices (S_q , R_q) and state-space partition line definitions are listed here⁵. Autonomous-mode 1, $U_1 \in [-2, 2] \times [-2, 2]$:

$$A_1 = \begin{bmatrix} -1 & 0.5 \\ -2 & -1 \end{bmatrix} \quad B_1 = \begin{bmatrix} 1 & 0 \\ 0 & 1 \end{bmatrix} \tag{62}$$

$$S_1 = \begin{bmatrix} 0.6 & 0 \\ 0 & 0.6 \end{bmatrix} \quad R_1 = \begin{bmatrix} 1 & 0 \\ 0 & 1 \end{bmatrix} \tag{63}$$

Autonomous-mode 2, $U_2 \in [-2, 2] \times [-2, 2]$:

$$A_2 = \begin{bmatrix} -1 & -2 \\ 0.5 & -0.1 \end{bmatrix} \quad B_2 = \begin{bmatrix} 1 & 0 \\ 0 & 1 \end{bmatrix} \tag{64}$$

$$S_2 = \begin{bmatrix} 1 & 0 \\ 0 & 1 \end{bmatrix} \quad R_2 = \begin{bmatrix} 1 & 0 \\ 0 & 1 \end{bmatrix} \tag{65}$$

Autonomous-mode 3, $U_3 \in [-2, 2] \times [-2, 2]$:

$$A_3 = \begin{bmatrix} -0.5 & -0.1 \\ -0.1 & -0.1 \end{bmatrix} \quad B_3 = \begin{bmatrix} 1 & 0 \\ 0 & 1 \end{bmatrix} \tag{66}$$

$$S_3 = \begin{bmatrix} 0.5 & 0 \\ 0 & 0.5 \end{bmatrix} \quad R_3 = \begin{bmatrix} 0.1 & 0 \\ 0 & 0.1 \end{bmatrix} \tag{67}$$

Autonomous-mode 4, $U_4 \in [-2, 2] \times [-2, 2]$:

$$A_4 = \begin{bmatrix} -0.5 & -3 \\ 0.5 & -1 \end{bmatrix} \quad B_4 = \begin{bmatrix} 1 & 0 \\ 0 & 1 \end{bmatrix} \tag{68}$$

$$S_4 = \begin{bmatrix} 0.5 & 0 \\ 0 & 0.5 \end{bmatrix} \quad R_4 = \begin{bmatrix} 0.1 & 0 \\ 0 & 0.1 \end{bmatrix} \tag{69}$$

Autonomous-mode 5, $U_5 \in [-2, 2] \times [-2, 2]$:

$$A_5 = \begin{bmatrix} -2 & -2 \\ 0.5 & -2 \end{bmatrix} \quad B_5 = \begin{bmatrix} 1 & 0 \\ 0 & 1 \end{bmatrix} \tag{70}$$

⁵Passenberg supplied the problem values through personal correspondence.

$$S_5 = \begin{bmatrix} 0.1 & 0 \\ 0 & 0.1 \end{bmatrix} \quad R_5 = \begin{bmatrix} 0.1 & 0 \\ 0 & 0.1 \end{bmatrix} \quad (71)$$

Autonomous-mode 6, $U_6 \in [-2, 2] \times [-2, 2]$:

$$A_6 = \begin{bmatrix} -0.1 & 0.2 \\ -2 & -2 \end{bmatrix} \quad B_6 = \begin{bmatrix} 1 & 0 \\ 0 & 1 \end{bmatrix} \quad (72)$$

$$S_6 = \begin{bmatrix} 8 & 0 \\ 0 & 8 \end{bmatrix} \quad R_6 = \begin{bmatrix} 1 & 0 \\ 0 & 1 \end{bmatrix} \quad (73)$$

Autonomous-mode 7, $U_7 \in [-2, 2] \times [-2, 2]$:

$$A_7 = \begin{bmatrix} -0.5 & -2 \\ 0.5 & -1 \end{bmatrix} \quad B_7 = \begin{bmatrix} 1 & 0 \\ 0 & 1 \end{bmatrix} \quad (74)$$

$$S_7 = \begin{bmatrix} 1 & 0 \\ 0 & 1 \end{bmatrix} \quad R_7 = \begin{bmatrix} 0.5 & 0 \\ 0 & 0.5 \end{bmatrix} \quad (75)$$

Autonomous-mode 8, $U_8 \in [-1, 1] \times [-1, 1]$:

$$A_8 = \begin{bmatrix} -0.5 & -1 \\ 5 & -0.5 \end{bmatrix} \quad B_8 = \begin{bmatrix} 1 & 0 \\ 0 & 1 \end{bmatrix} \quad (76)$$

$$S_8 = \begin{bmatrix} 0.1 & 0 \\ 0 & 0.1 \end{bmatrix} \quad R_8 = \begin{bmatrix} 0.1 & 0 \\ 0 & 0.1 \end{bmatrix} \quad (77)$$

Autonomous-mode 9, $U_9 \in [-2, 2] \times [-2, 2]$:

$$A_9 = \begin{bmatrix} -0.1 & 0.5 \\ -0.5 & -0.2 \end{bmatrix} \quad B_9 = \begin{bmatrix} 1 & 0 \\ 0 & 1 \end{bmatrix} \quad (78)$$

$$S_9 = \begin{bmatrix} 10 & 0 \\ 0 & 10 \end{bmatrix} \quad R_9 = \begin{bmatrix} 1 & 0 \\ 0 & 1 \end{bmatrix} \quad (79)$$

Autonomous-mode 10, $U_{10} \in [-10, 10] \times [-1, 1]$ (u_2 dummy variable defined for consistency with other mode parameter definitions, has no effect on dynamics or cost):

$$A_{10} = \begin{bmatrix} -4 & 2 \\ 0 & -4 \end{bmatrix} \quad B_{10} = \begin{bmatrix} 1 & 0 \\ 1 & 0 \end{bmatrix} \quad (80)$$

$$S_{10} = \begin{bmatrix} 2 & 0 \\ 0 & 2 \end{bmatrix} \quad R_{10} = \begin{bmatrix} 1 & 0 \\ 0 & 0 \end{bmatrix} \quad (81)$$

Autonomous-mode 11, $U_{11} \in [-2, 2] \times [-2, 2]$:

$$A_{11} = \begin{bmatrix} -1 & 1 \\ 1 & -2 \end{bmatrix} \quad B_{11} = \begin{bmatrix} 1 & 0 \\ 0 & 1 \end{bmatrix} \quad (82)$$

$$S_{11} = \begin{bmatrix} 2 & 0 \\ 0 & 2 \end{bmatrix} \quad R_{11} = \begin{bmatrix} 1 & 0 \\ 0 & 1 \end{bmatrix} \quad (83)$$

Next, the lines separating the state-space regions are defined.

$$x_1 = -3, \quad x_2 \in [-4, -2] \quad (84)$$

$$x_1 = -5, \quad x_2 \in [-7, -3] \quad (85)$$

$$x_2 = -x_1 - 14, \quad x_1 \in [-7, -6] \quad (86)$$

$$x_2 = -7, \quad x_1 \in [-10, 5] \quad (87)$$

$$x_2 = -0.5x_1 - 5.5, \quad x_1 \in [-10, -3] \quad (88)$$

$$x_2 = -4, \quad x_1 \in [-3, 5] \quad (89)$$

$$x_2 = 2x_1 - 4, \quad x_1 \in [-1.5, 0] \quad (90)$$

$$x_2 = 0, \quad x_1 \in [-10, -5] \quad (91)$$

$$x_2 = -x_1 - 5, \quad x_1 \in [-5, -3] \quad (92)$$

$$x_2 = -2, \quad x_1 \in [-3, 0] \quad (93)$$

$$x_2 = -x_1 - 2, \quad x_1 \in [0, 2] \quad (94)$$

$$x_2 = x_1 - 2, \quad x_1 \in [0, 4] \quad (95)$$

$$x_2 = 2, \quad x_1 \in [4, 5] \quad (96)$$

$$x_2 = 0.8x_1 + 4, \quad x_1 \in [-5, 0] \quad (97)$$

$$x_2 = -0.5x_1 + 4, \quad x_1 \in [0, 4] \quad (98)$$

ACKNOWLEDGEMENTS

This work was partially supported by the Office of Naval Research, and National Science Foundation grants IIS-0905593, CNS-0910988 and CNS-1035914. We would like to thank Tim Caldwell and Professor Murphey for supplying us with the mode 2 and 3 skid-steered vehicle dynamics as well as the vehicle's physical parameters and Benjamin Passenberg for providing their 11-region system problem data and results. Professor Borrelli kindly provided access to code and information on the spring-mass system. Finally, we would like to thank Professors Egerstedt and Wardi as well as Philip

Twu who supplied essential details of the two-tank and mobile robot problems.

REFERENCES

- [1] F. Borrelli, A. Bemporad, and M. Morari, *Predictive Control for Linear and Hybrid Systems*. Cambridge, 2011.
- [2] M. Kvasnica, P. Grieder, and M. Baotić, “Multi-Parametric Toolbox (MPT),” 2004. [Online]. Available: <http://control.ee.ethz.ch/~mpt/>
- [3] IBM Corporation, “IBM ILOG CPLEX Optimizer 12.3,” 2012. [Online]. Available: <http://www-01.ibm.com/software/integration/optimization/cplex-optimizer>
- [4] Y. Wardi, P. Twu, and M. Egerstedt, “On-line Optimal Timing Control of Switched Systems,” in *49th IEEE Conference on Decision and Control (CDC)*, Atlanta, GA, 2010, pp. 2137 – 2142.
- [5] Y. Wardi and M. Egerstedt, “Algorithm for Optimal Mode Scheduling in Switched Systems,” in *Proceedings of the American Control Conference*, Montreal, Canada, 2012.
- [6] B. Passenberg, P. Caines, M. Sobotka, O. Stursberg, and M. Buss, “The minimum principle for hybrid systems with partitioned state space and unspecified discrete state sequence,” in *49th IEEE Conference on Decision and Control (CDC)*, Dec. 2010, pp. 6666 – 6673.
- [7] B. Passenberg, M. Sobotka, O. Stursberg, M. Buss, and P. Caines, “An algorithm for discrete state sequence and trajectory optimization for hybrid systems with partitioned state space,” in *49th IEEE Conference on Decision and Control (CDC)*, Dec. 2010, pp. 4223 – 4229.
- [8] S. C. Bengea and R. A. DeCarlo, “Optimal control of switching systems,” *Automatica*, vol. 41, no. 1, pp. 11 – 27, 2005. [Online]. Available: <http://dx.doi.org/10.1016/j.automatica.2004.08.003>
- [9] S. Wei, K. Uthaichana, M. Žefran, R. DeCarlo, and S. Bengea, “Applications of numerical optimal control to nonlinear hybrid systems,” *Nonlinear Analysis: Hybrid Systems*, vol. 1, pp. 264 – 279, 2007.
- [10] K. Uthaichana, R. A. DeCarlo, S. C. Bengea, S. Pekarek, and M. Zefran, “Hybrid optimal theory and predictive control for power management in hybrid electric vehicle,” *Journal of Nonlinear Systems and Applications*, vol. 2, no. 1 -2, pp. 96 – 110, 2011.
- [11] R. T. Meyer, R. A. DeCarlo, P. H. Meckl, C. Doktorcik, and S. Pekarek, “Hybrid model predictive power flow control of a fuel cell-battery vehicle,” in *Proceedings of the American Control Conference*, San Francisco, CA, United states, 2011, pp. 2725 – 2731.
- [12] S. Wei, M. Zefran, K. Uthaichana, and R. A. DeCarlo, “Hybrid Model Predictive Control for Stabilization of Wheeled Mobile Robots Subject to Wheel Slippage,” in *ICRA '07, 2007*, pp. 2373 – 2378.
- [13] J. Neely, S. Pekarek, and R. DeCarlo, “Hybrid optimal-based control of a boost converter,” in *IEEE Applied Power Electronics Conference and Exposition*, 2009, pp. 1129 – 1137.
- [14] F. Oettmeier, J. Neely, S. Pekarek, R. DeCarlo, and K. Uthaichana, “MPC of switching in a boost converter using a hybrid state model with a sliding mode observer,” *IEEE Transactions on Industrial Electronics*, vol. 56, no. 9, pp. 3453–3466, 2009.
- [15] J. Neely, S. Pekarek, R. DeCarlo, and N. Vaks, “Real-time hybrid model predictive control of a boost converter with constant power load,” in *Conference Proceedings - IEEE Applied Power Electronics Conference and Exposition - APEC*, Palm Springs, CA, United states, 2010, pp. 480 – 490. [Online]. Available: <http://dx.doi.org/10.1109/APEC.2010.5433628>
- [16] J. Neely, R. DeCarlo, and S. Pekarek, “Real-time model predictive control of the cuk converter,” in *2010 IEEE 12th Workshop on Control and Modeling for Power Electronics, COMPEL 2010*, Boulder, CO, United states, 2010. [Online]. Available: <http://dx.doi.org/10.1109/COMPEL.2010.5562383>
- [17] S. Mariéthoz, S. Almér, M. Bâja, A. G. Beccuti, D. Patino, A. Wernrud, J. Buisson, H. Cormerais, T. Geyer, H. Fujioka, U. T. Jönsson, C.-Y. Kao, M. Morari, G. Papafotiou, A. Rantzer, and P. Riedinger, “Comparison of Hybrid Control Techniques for Buck and Boost DC-DC Converters,” *IEEE Transactions on Control Systems Technology*, vol. 18, no. 5, pp. 1126 – 1145, September 2010.
- [18] T. Caldwell and T. Murphey, “Relaxed optimization for mode estimation in skid steering,” in *2010 IEEE International Conference on Robotics and Automation (ICRA 2010)*, Piscataway, NJ, USA, 2010, pp. 5423 – 5428. [Online]. Available: <http://dx.doi.org/10.1109/ROBOT.2010.5509356>
- [19] —, “Switching mode generation and optimal estimation with application to skid-steering,” *Automatica*, vol. 47, no. 1, pp. 50 – 64, January 2011. [Online]. Available: <http://dx.doi.org/10.1016/j.automatica.2010.10.010>
- [20] S. C. Bengea and R. A. DeCarlo, “Optimal Control of a Two-Switched Linear System,” *Journal of Control Engineering and Applied Informatics*, vol. 5, no. 2, pp. 11 – 16, December 2003.
- [21] S. C. Bengea, K. Uthaichana, M. Zefran, and R. A. DeCarlo, *The Control Handbook: Advanced Methods*, 2nd ed. CRC Press, 2011, ch. Optimal Control of Switching Systems via Embedding into Continuous Optimal Control Problem, pp. 31–1 – 31–23.
- [22] S. C. Bengea and R. A. DeCarlo, “Optimal and Suboptimal

- Control of Switched Systems,” in *42nd IEEE Conference on Decision and Control*, Dec. 2003, pp. 5925 – 5300.
- [23] R. T. Meyer, R. A. DeCarlo, P. H. Meckl, and S. Pekarek, “Hybrid model predictive power management of a fuel-cell battery vehicle,” *accepted Asian Journal of Control*, 2012.
- [24] G. Matthews and R. DeCarlo, “Decentralized Tracking for a Class of Interconnected Nonlinear Systems Using Variable Structure Control,” *Automatica*, vol. 24, no. 2, pp. 187 – 193, March 1988.
- [25] X. Xu and P. J. Antsaklis, “Optimal Control of Switched Systems: New Results and Open Problems,” in *Proceedings of the American Control Conference*, Chicago, IL, 2000, pp. 2683 – 2687.
- [26] P. Reidinger, C. Zanne, and F. Kratz, “Time Optimal Control of Hybrid Systems,” in *Proceedings of the American Control Conference*, San Diego, CA, 1999, pp. 2466 – 2470.
- [27] P. Reidinger, C. Kratz, F. Lung, and C. Zanne, “Linear Quadratic Optimization for Hybrid Systems,” in *Proceedings of the American Control Conference*, 1999, pp. 3059–3064.
- [28] R. Meyer, R. A. DeCarlo, and M. Žefran, “Matlab toolbox for hybrid optimal control,” 2012. [Online]. Available: http://robotics.ece.uic.edu/hocp_code
- [29] S. Richter and R. DeCarlo, “Continuation Methods: Theory and Applications,” *IEEE Transactions on Automatic Control*, vol. 28, pp. 660 – 665, 6 1983.
- [30] J. Neely, “Real-Time Hybrid Model Predictive Control of Switched DC-DC Converters,” Ph.D. dissertation, Purdue University, 2010.
- [31] M. Žefran, J. Desai, and V. Kumar, “Continuous motion plans for robotic systems with changing dynamic behavior,” in *Robotic motion and manipulation*, J.-P. Laumond and M. Overmars, Eds. Wellesley, MA: A K Peters, 1997, pp. 113 – 128.
- [32] Y. Wang and S. Boyd, “Fast model predictive control using online optimization,” *IEEE Transactions on Control Systems Technology*, vol. 18, no. 2, pp. 267 – 278, 2010. [Online]. Available: <http://dx.doi.org/10.1109/TCST.2009.2017934>